JOURNAL OF MATERIALS SCIENCE 20 (1985) 1407–1418

Microstructure and sintering kinetics of highly reactive ZrO_2–Y_2O_3 ceramics

M. A. C. G. VAN DE GRAAF, J. H. H. TER MAAT, A. J. BURGGRAAF
Twente University of Technology, Department of Chemical Engineering, Laboratory of Inorganic Chemistry and Materials Science, PO Box 217, 7500 AE Enschede, The Netherlands

Ultra-fine stabilized zirconia powders, which only contain extremely small aggregates were prepared. The control of agglomerates and aggregates in these powders is of utmost importance in order to obtain highly sinter-reactive ceramics. The very small aggregates appear to be the smallest microstructural units which determine the ultimate packing situation after compaction. Resulting green microstructures and sintering behaviour were studied extensively. The sintering process is seen to proceed via several stages of microstructural development. During the most important stage, where the ceramic material approaches full density, the observed occurrence of abnormal grain growth strongly influences the ultimate grain size. The extent of abnormal growth is highly dependent on aggregate sizes present in the starting powder.

1. Introduction

In the application of stabilized zirconia as a solid electrolyte in electronic devices such as sensors and oxygen pumps, in addition to electrical demands [1], the material has to meet certain requirements concerning ceramic microstructure. The ceramic material has to be impervious to gases and, furthermore, mechanical strength and toughness must be sufficiently high in order to prevent breakdown of the device during use at elevated temperatures.

As was discussed previously [2–4], highly sinter-reactive powders enable the production of dense ceramics with a very small grain size ($< 0.5\ \mu m$). In particular yttria stabilized zirconia powders prepared from metal alkoxides [3, 4] give good results and produce ultra-fine grained ceramics with enhanced mechanical strength [5]. The densification of stabilized zirconia ceramics at relatively low temperatures [2] is only possible when a very homogenous microstructure, i.e. a highly uniform packing of ultra-fine crystallites in the green compact is present [3, 6].

In the case of ultra-fine ceramic powders from metal alkoxides the product is formed by hydrolysis–precipitation of the precursor solution in water [4, 7, 8]. In order to prevent the formation of strong agglomerates the precipitated hydrous gel has to be treated in such a way so that a low density gel with a minimal degree of internal cross-linking is formed [3, 8, 10]. According to Sheinfain *et al.* [11], Stas' *et al.* [12] and Veiga *et al.* [13], gels which were aged in different liquids mutually show rather drastic differences in the pore volume after drying at 120° C. Ageing in water leads to the formation of very dense xerogels, whereas ageing in organic solvents (e.g. 2-propanol) produces highly porous dry gels. Rijnten [9] and Dell *et al.* [14] suggest that adsorbed water promotes low temperature sintering of gel-derived oxides. In the case of alkoxide-derived gels, both phenomena mentioned above may enhance the formation of dense and, consequently, strong agglomerates during thermal decomposition.

In the present work special precautions were taken during synthesis in order to allow complete removal of free water from hydrous zirconia precipitates, prior to drying and calcining, which produces powders with improved compaction and sintering behaviour. In some recent papers [4, 6] the microstructural development during compaction of these yttria stabilized zirconia powders

0022–2461/85 $03.00 + .12

was discussed in detail. The work reported here briefly reviews compaction behaviour, while a more extensive study concerning sintering behaviour is presented. Special attention will be paid to the interaction of grain growth and densification during the sintering process and the consequences of these phenomena on the microstructural development and resulting grain sizes.

2. Experimental details

2.1. Sample preparation

Metal alkoxide precursors: Zr–t–amyloxide; $Zr(OC_5H_{11})_4$; and yttrium isopropoxide, $Y(OC_3H_7)_3$, were synthesized as described by Bradley *et al.* [15] and Brown *et al.* [16]. 17% yttria stabilized zirconia, $Zr_{0.83}Y_{0.17}O_{1.915}$, was prepared by hydrolysis of a mixed solution of the alkoxides and subsequent decomposition of the hydroxide–gel precipitate [3].

In order to achieve powders with optimal compaction and sintering properties, the following conditions must be fulfilled: (i) a maximum degree of dispersion has to be accomplished during hydrolysis; and (ii) free water has to be totally removed from the surface of the gelatinous precipitate prior to drying and thermal decomposition. To meet these conditions, hydrolysis and gel washing procedures as previously reported [3] were modified as follows: a very dilute (0.2 M) alkoxide solution in benzene was added dropwise to a large excess of water, molar ratio $H_2O \div$ metal = 250. After hydrolysis, the precipitate was laundered with water three times to complete the hydrolysis reaction and in order to remove organic solvents. Washing was repeated three times with 2-propanol for the total removal of water from the hydrous gel. Prior to each washing step, the filtered gel was ball-milled as a viscous slurry (4 M) to facilitate subsequent dispersion. All washing steps were performed with highly diluted ($\simeq$0.1 M) gel dispersions. Hydrolysis and washing procedures were carried out in a baffled vessel reactor (Fig. 1a) as described by Lyons [17]. During hydrolysis, the reactor was equipped with a dispersion turbine (Fig. 1b), which provides a high degree of dispersion of the hydrolysing material. Water and alcohol washing steps were carried out using a high energy disc turbine (Fig. 1c). This turbine, which was operated at 1000 rpm, provides an extremely high liquid flow, which enables maximum removal of water out of the gel structure. After the last washing step, the gel was dried, ball-milled and calcined at 650° C. Powder compacts were pressed isostatically at pressures of up to 500 MPa. Sintering took place at temperatures between 700 and 1500° C in air.

2.2 Characterization

X-ray fluorescence spectrometry, using a Philips PW 1410 spectrometer, was used for the analysis of overall composition and purity [18]. Powder compaction behaviour was investigated by measuring the changes in densification with increasing isostatic pressure as described by Niesz *et al.* [19]. Specific surface areas of the powders were determined according to the BET method using the equipment as reported by Bosch *et al.* [20]. Nitrogen adsorption and desorption isotherms were measured at 77 K by means of a Carlo Erba Sorptomatic Series 1800 instrument. Pore size distributions and pore volumes were calculated from the desorption branch of the hysteresis loops, according to the method described by Dollimore *et al.* [21]. The total pore volume data so determined, were compared with pore volume values calculated from the overall density values, measured by means of the Archimedes method. Crystallite sizes as a function of heat treatment temperature were determined by means of X-ray line broadening measurement [22], using a Philips X-ray diffractometer PW 1370 with Cu$K\alpha$-radiation. A Jeol 200 CT transmission electron microscope was used for direct observation of grain sizes in the region < 200 nm. Grain growth in the region > 200 nm was observed using a Jeol JSM U3 scanning electron microscope.

3. Results and discussion

3.1. Powder characteristics

X-ray fluorescence analysis revealed a chemical composition $Zr_{0.835}Y_{0.165}O_{1.9175}$, which is a value near to the nominal composition. The powder contained traces of contaminants: $Al_2O_3 <$ 100 ppm; $SiO_2 < 300$ ppm; and $C < 500$ ppm. The calcined powder showed a specific surface area as high as 90 $m^2\,g^{-1}$. The average crystalline size of 7.8 nm, as calculated from X-ray line broadening data showed good agreement with transmission electron microscope observations (Fig. 2).

3.2. Microstructural development during compaction

As previously reported in more detail [4], the alkoxide powders under investigation are built up

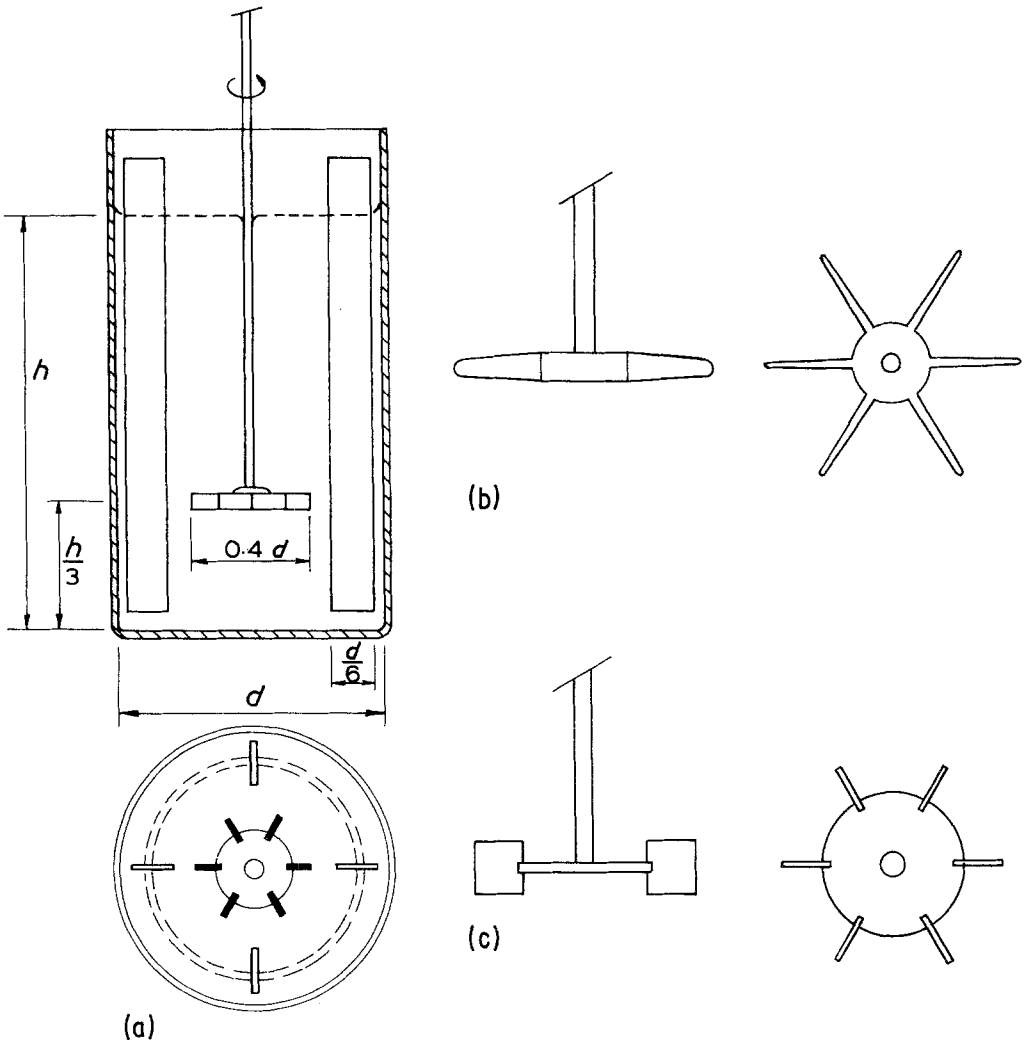

Figure 1 (a) baffled vessel hydrolysis and washing reactor, (b) dispersion turbine, (c) disc turbine.

from three microstructural elements: (a) primary *crystallites* ($\bar{G}_{cr} = 7.8$ nm), which are closely packed into (b) very small and strong aggregates ($\bar{d}_{aggr} \simeq 20$ nm); and (c) a large number of aggregates mutually clustered to form weak and highly porous *agglomerates* (relative agglomerate density = 23%).

Stepwise compaction, with increasing isostatic pressure, shows a densification behaviour as illustrated in Fig. 3. The intersection between two linear parts of this curve represents the average compression strength (30 MPa) of the agglomerates. At pressures < 30 MPa, densification of the compact takes place merely by fragmentation and rearrangement of the agglomerates without a change of their internal microstructure. At pressures exceeding 30 MPa, however, the agglomerate fragments are being compressed, which causes changes in their internal microstructure.

Fig. 4 schematically represents an idealized picture of the compaction sequence, whereas Fig. 5 shows a pore size distribution curves as measured for the four stages ($P = 4$, 8, 95 and 400 MPa respectively) of microstructural development. At pressures below 30 MPa (Figs. 4a and 4b) a fraction of large pores ($\bar{r}_p > 50$ nm) is present, together with a relatively sharp distribution of much smaller pores (the smaller pores being located within the agglomerates) whereas the fraction of coarser pores is caused by inter-agglomerate cavities, due to the presence of agglomerate fragments at pressures < 30 MPa. The volume contribution of the larger pores to the total pore volume, as well as their size, decrease on

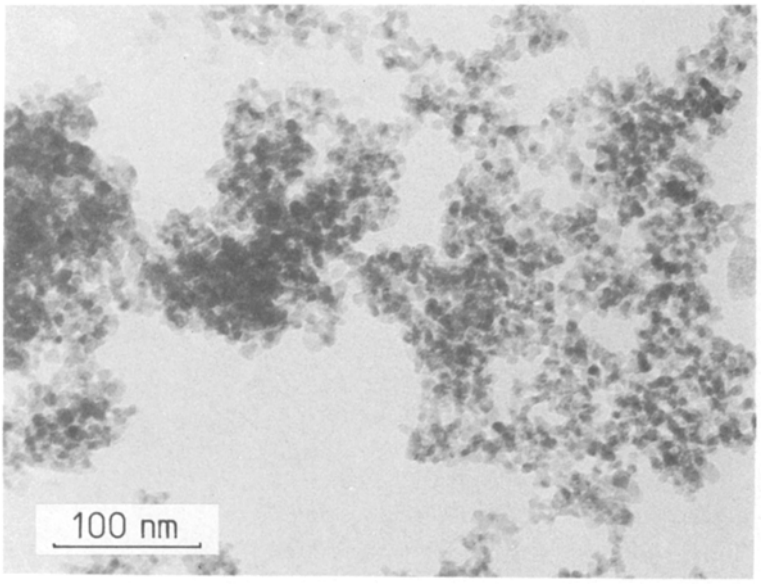

Figure 2 Transmission electron micrograph of an alkoxide powder sample calcined at 650° C.

increasing pressure in the region $0 < P < 30$ MPa (Fig. 5b). As can be seen in Figs. 5c and d, at pressures exceeding 30 MPa inter-agglomerate pores have disappeared, whereas the size of the inter-aggregate pores decreases on increasing pressure as a result of aggregate rearrangement. Because of their high density and high strength these aggregates merely rearrange, without their internal microstructure being affected. Finally, at $P = 400$ MPa (Figs. 4d and 5d) this results in a rather narrow size distribution of inter-aggregate pores ($\bar{r}_p = 4.3$ nm) and, in addition, a small shoulder ($\bar{r}_p = 2$ nm) originating from the pores within these aggregates. As will be shown later, the existence of these small aggregates strongly influences microstructural development during the first stages of sintering.

As was shown in a previous paper [3] synthesis of stabilized zirconia powders from metal alkoxides, following the conventional route, produces relatively sinter-reactive powders. These powders, however, consist of dense ($\rho_{rel} = 60\%$) and fairly strong (compression strength = 110 MPa) agglomerates, resulting in the persistence of rather coarse pores during compaction. The actual powders which, as described before, were prepared according to improved hydrolysis and washing conditions, only contain very weak (compression strength 30 MPa) and highly porous agglomerates ($\rho_{rel} = 23\%$) [4]. As will be shown, this leads to a

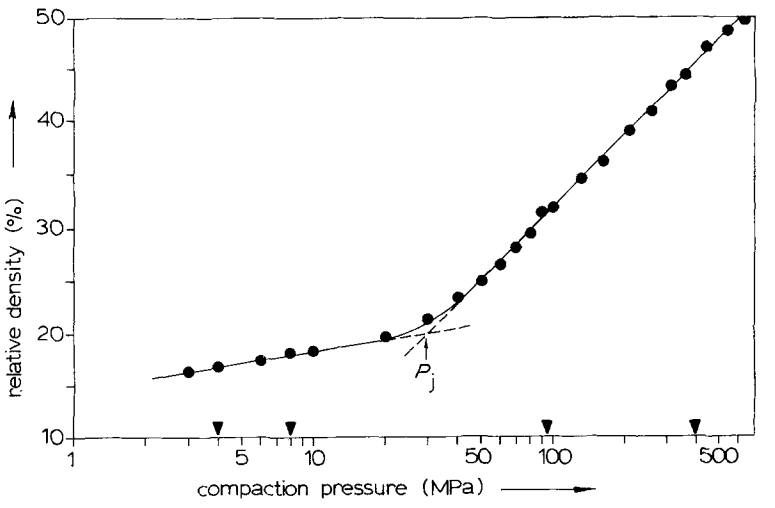

Figure 3 Densification behaviour during isostatic compaction.

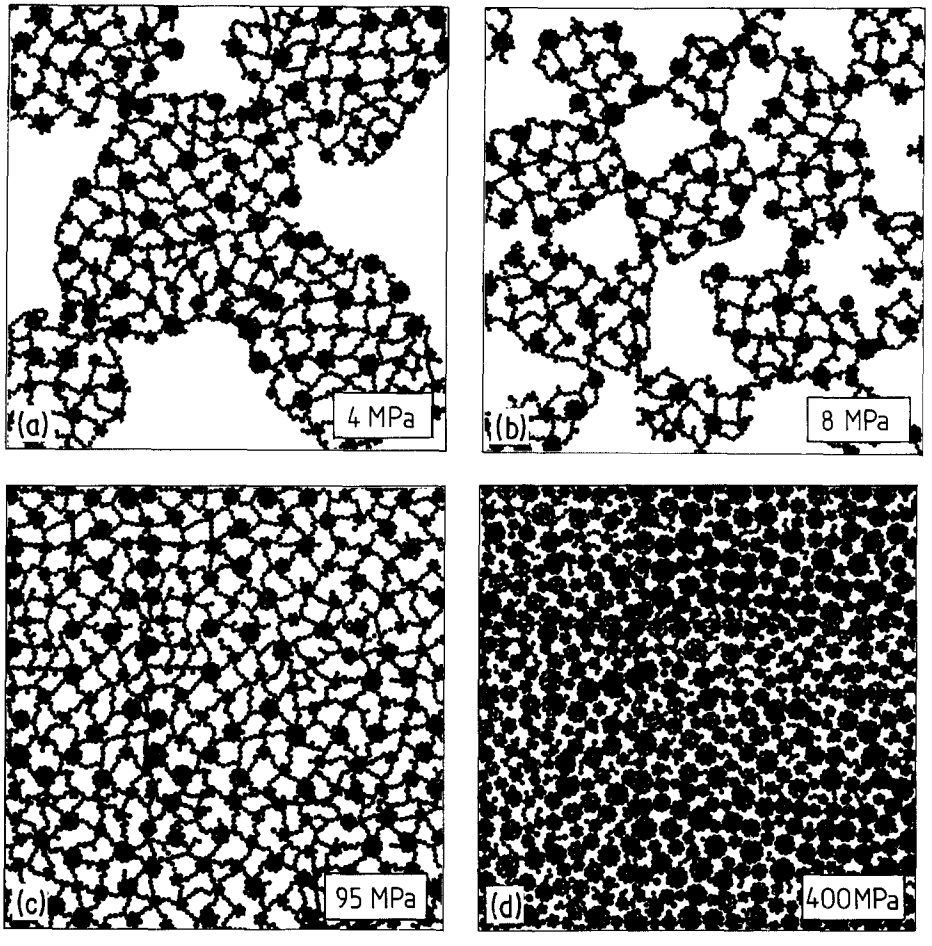

Figure 4 Schematic representation of microstructural development during the different stages of the compaction process at pressures of (a) 4 MPa, (b) 8 MPa, (c) 95 MPa and (d) 400 MPa.

considerable improvement in sinter-reactivity.

3.3. Development of microstructural parameters during sintering

Densification, the development of pore sizes and grain growth at different sintering temperatures are represented in Figs. 6 to 8. At temperatures below 1100° C, sintering involves pore growth and only slight densification. Above 1100° C a different behaviour is observed: pore shrinkage occurs and densification rapidly accelerates towards the final 97% density. The onset of pore shrinkage corresponds with the start of fast densification (Figs. 6 and 7).

Grain growth behaviour may be interpreted by means of the kinetic theory developed by Brook [23] in which growth equations of the general form are used:

$$G^n - G_0^n \propto \frac{D}{T} \times t \tag{1}$$

where n is a constant for a given growth mechanism; D is the diffusion constant of the slowest ion; G_0 and G are the starting grain size for the actual mechanism and the grain size resulting from grain growth at a temperature T during time t, respectively. These grain growth equations may be used for isothermal grain growth studies. In our investigation microstructural development, including grain growth, was studied by carrying out sintering experiments at several temperatures, with constant sintering times. For this reason Equation 1 is transformed making use of the temperature dependence relation for the diffusion constant:

$$D = D_0 \exp -\frac{\Delta E}{RT} \tag{2}$$

from which:

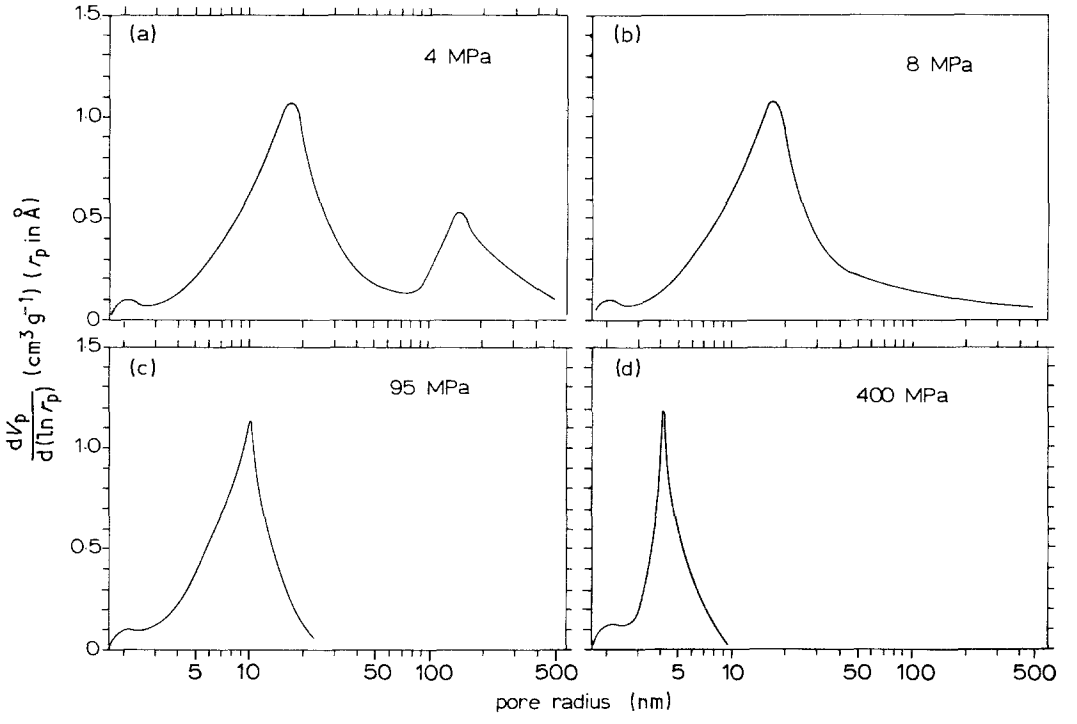

Figure 5 Pore size distribution curves determined from gas desorption measurements. Pressures correspond with values indicated in Figs. 3 and 4.

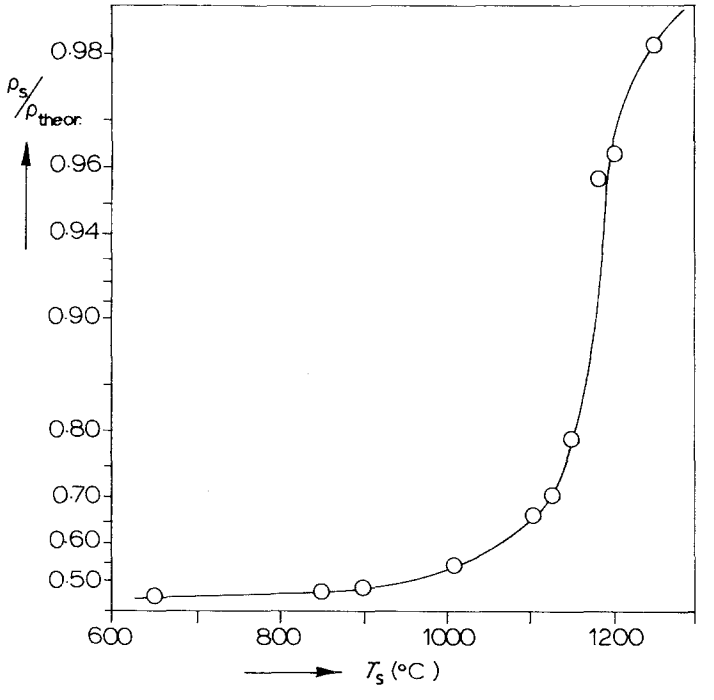

Figure 6 Densification during sintering of compacted (400 MPa) alkoxide ZY 17 powder.

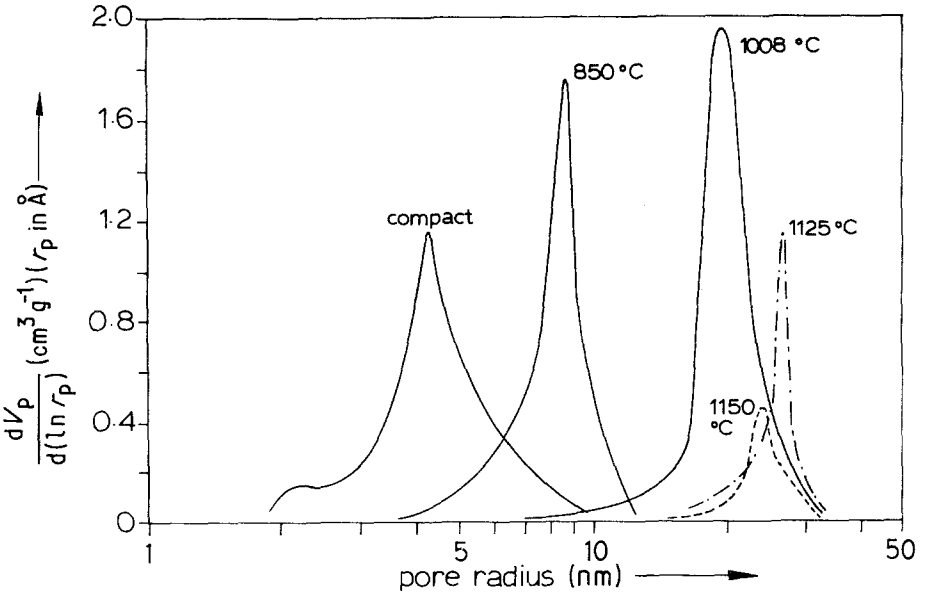

Figure 7 Development of pore size distribution during the sintering process.

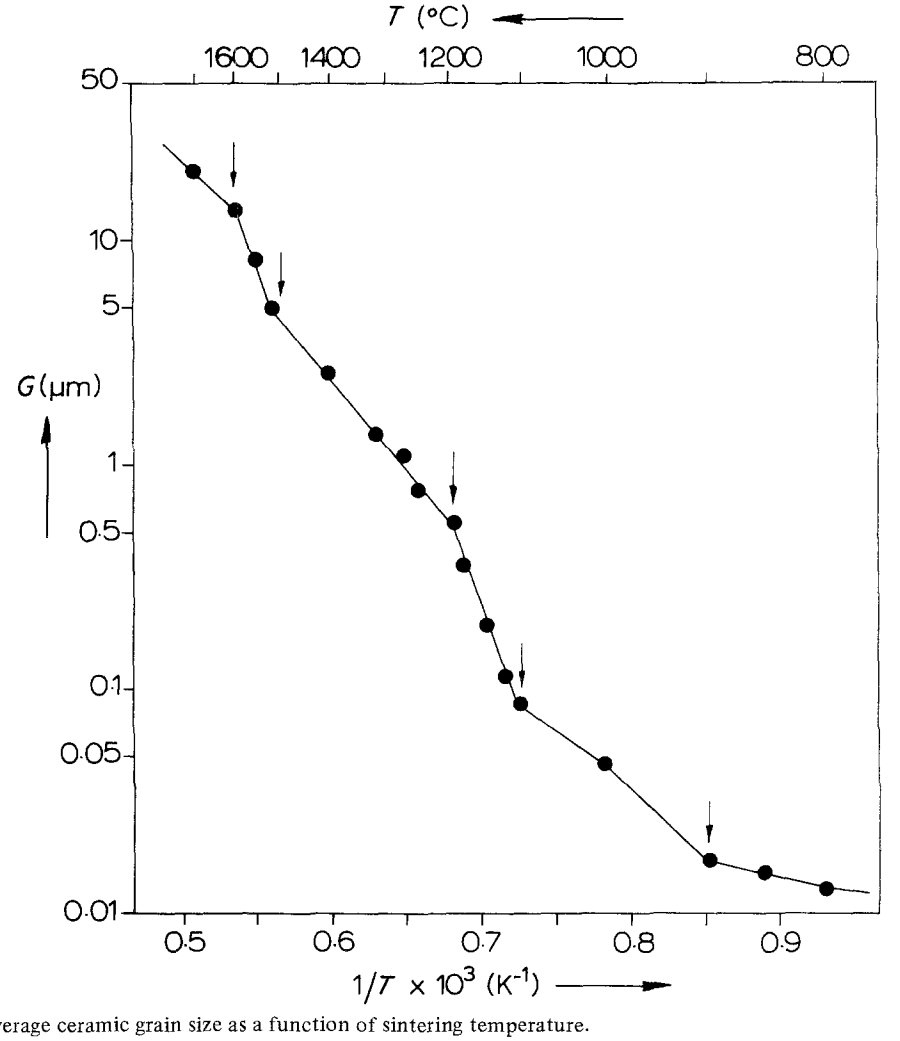

Figure 8 Average ceramic grain size as a function of sintering temperature.

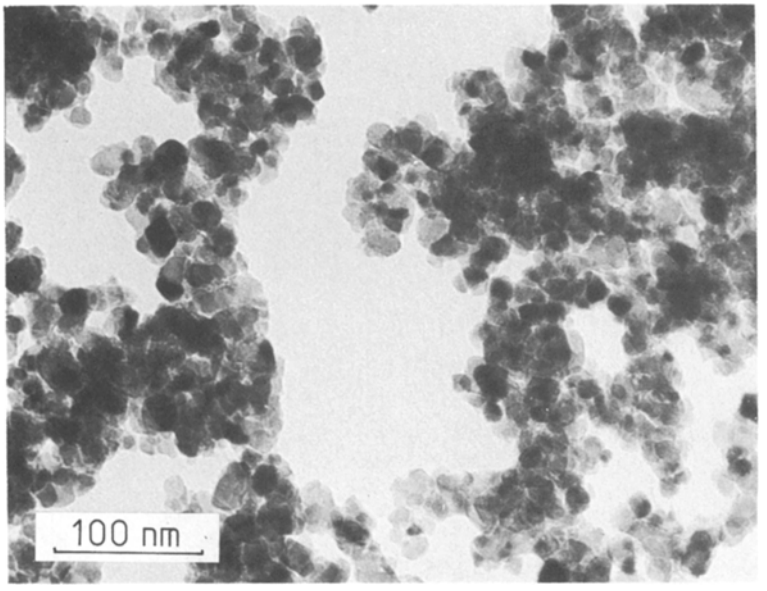

Figure 9 Transmission electron micrograph of an alkoxide powder sample, heat treated at 850° C.

$$\ln (G^n - G_0^n) \propto -\frac{\Delta E}{RT} + \ln D_0 + \ln t - \ln T \quad (3)$$

With the condition: $G \gg G_0$; and t is constant; D_0 is constant (no compositional changes), for each small temperature interval within the region of one single grain growth mechanism. Equation 3 then becomes:

$$\ln G \propto -\frac{\Delta E}{nRT} + \text{constant}. \quad (4)$$

For the above conditions, with a fixed value of n, Equation 4 describes grain growth within the temperature limits of an operating growth mechanism. Though the condition $G \gg G_0$, as will be shown later, is not completely fulfilled in each temperature region studied, a distinct change in the slope of a $\ln G$ against $1/T$ plot is indicative of a change in the acting grain growth mechanism. As is shown in Fig. 8, grain growth follows a quite complex pattern. A classification into six temperature regions of grain growth kinetics can be made, the transition temperatures being 900, 1100, 1200, 1500 and 1600° C.

Below the first transition temperature (900° C), the sintering can be attributed to the presence of small ($\bar{d} < 20$ nm) aggregates mentioned before. The observed increase in grain size in this temperature region, is caused exclusively by grain growth *within* these small aggregates. The relatively regular and dense internal packing situation in these small aggregates provides a large number of necks, formed during calcining, between the primary crystallites. As was shown in a previous paper, such packing situations lead to fast sintering and the achievement of full density at very low temperatures [2]. *Between* the aggregates, this advantageous situation does not exist: here the number of contact points per unit volume is very much lower. As a consequence mutual sintering between these aggregates is negligible in this temperature region. Hence sintering will be mainly restricted to the internal aggregate structure. In the course of this process, the pore volume within the aggregates is transported towards the surface of the aggregates. This results in complete densification of the aggregates, which is confirmed by the disappearance of intra-aggregate pores and enlarged inter-aggregate pores (Fig. 7), whereas the overall compact densification is negligible (Fig. 6).

After calcining (650° C), the average aggregate diameter $\bar{d}_{aggr} \simeq 20$ nm and the relative internal aggregate density $\rho_{rel} = 45\%$ (pore fraction $\epsilon = 0.55$) [4]. As discussed above, after sintering at 900° C, these aggregates have completely densified. Making use of the simple geometrical relation:

$$\bar{d}_{900} = \bar{d}_{aggr} \times (1 - \epsilon)^{1/3} \quad (5)$$

the average aggregate size $\bar{d}_{900}$ after sintering at 900° C is calculated to be 15.3 nm. This value is close enough to the average crystallite size $\bar{G}_{900} = 17.3$ nm, measured after sintering at 900° C (Fig. 8), to conclude that the aggregates have densified to "single crystallites". The result of this important first stage of microstructural development is affirmed by the transmission electron micrograph of a sample, sintered at 850° C (Fig. 9). This

photograph shows both large crystals ($\bar{G} = 15$ to 20 nm), resulting from the completely densified aggregates and some remaining crystallites, experiencing an unfavourable packing situation in the uncompacted powder.

In the temperature region $900 < T < 1100^\circ$ C grain growth accelerates. After complete densification of the aggregates, a new stage in grain growth consequently implies growth of the large crystals, originating from these densified aggregates. In previous work on a related materials system [2] we reported growth kinetics with $n = 3$ in the same temperature region, a value which was attributed to normal grain growth. Since materials system and grain sizes are comparable, the same grain growth kinetics are to be expected in the actual material.

According to Brook [23] normal grain growth can be divided into two classes where: (a) grain boundary velocity itself is the rate controlling process; and (b) migration of the pores, attached to the grain boundary, is rate controlling. In the greater part of the temperature region concerned, most of the original porosity is still present (Fig. 6), whereas grains and pores grow simultaneously (Fig. 7 and 8) in the entire region. The cause of this simultaneous growth is, that in cases of normal grain growth pores remain attached to the moving grain boundary and will coalesce as small grains are consumed by larger grains [23, 24]. The pores can be expected to move along by surface diffusion considering the low temperatures and small grain and pore sizes involved at this stage of microstructural development.

In the course of normal grain growth, where pores migrate by way of surface diffusion, the observed simultaneous grain and pore growth normally lead to a shift in the rate controlling process from boundary mobility control to pore mobility control as pore and grain sizes increase [25]. Applying Equation 4, and considering the common assumption that $\Delta E/n$ is lower for surface diffusion than for diffusion across the boundary, the shift in the rate controlling process should imply a decrease in the slope of a $\ln G$ against $1/T$ graph at higher temperatures in this region. Although only little grain size data are available in the temperature region under discussion, the perceptible decrease in the slope towards the higher temperatures (Fig. 8), in combination with the microstructural development observed, provide supporting evidence for the proposed growth kinetics.

The sintering behaviour at higher temperatures ($T > 1100^\circ$ C) exhibits several different stages of grain growth as well. In particular the temperature region between 1100 and 1200° C will be discussed in more detail. As can be seen from Figs. 6 and 8, $\geqslant 95\%$ density is reached below 1200° C, whereas grain growth accelerates strongly in this area. Hence, this stage of microstructural development is very important for ceramic processing. The steep increase in the grain growth rate is indicative of abnormal grain growth occuring at this stage. Abnormal grain growth may originate from two sources: (a) The grain size distribution of the starting material may contain grains with sizes substantially exceeding the average grain size. Such grains may be the starting points of exaggerated grain growth [26]; and (b) Systems undergoing normal grain growth with mobile pores attached to the grain boundary may ultimately give rise to abnormal grain growth as pore velocities are more strongly dependent on pore size than the boundary velocities are on grain size [25]. In the course of the process where grain growth is accompanied by pore growth, pores may separate from the grain boundaries and abnormal grain growth may start. The latter growth mechanism, where the pore mobility finally controls the grain growth rate, has been established in the preceding stage. Ultimately this mechanism may lead to coincident local situations, where large pores are attached to the boundaries of large grains in a relatively fine-grained boundary. This ends in the grain boundary abandoning the pore and the grain starts growing uninhibited. Abnormal grain growth is, therefore, the logical consequence of normal grain growth in a system with mobile, growing pores.

The assumed appearance of abnormal grain growth in the temperature region $1100 < T < 1200^\circ$ C may be supported by applying Equation 3 and using the connected theoretical value $n = 1$. Fig. 10 shows a plot of $\ln (G - G_0)$ against $1/T$ for a value $G_0 = 50$ nm. This value, at which the curve of Fig. 8 starts to deviate perceptively, indicating the onset of pore control, has been chosen more or less arbitrarily (it should be noted that the exact choice of the G_0 value only influences the $\ln (G - G_0)$ value for $T = 1100^\circ$ C appreciably and, consequently, not the slope of the graph). From Fig. 10 a value for ΔE of 450 kJ mol^{-1} is estimated for $n = 1$. It should be noted, that plotting of the data, using $n = 2$ to 4 all yield physically impossible high values for ΔE, thus excluding

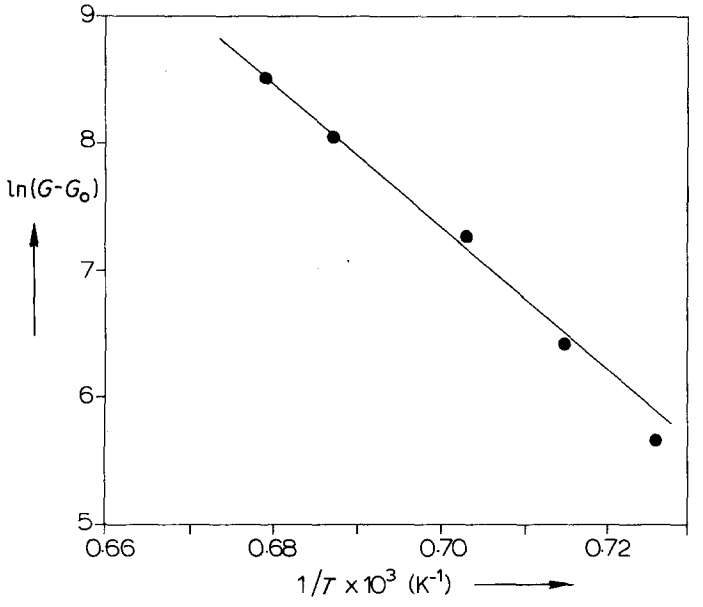

Figure 10 ln $(G - G_0)$ against $1/T$ plot for grain growth in the temperature region $1100 < T < 1200^\circ$ C.

other grain growth mechanisms. From the above, mainly circumstantial evidence, we tentatively conclude abnormal grain growth to be the operating mechanism in the region $1100 < T < 1200^\circ$ C.

The stage 1200–1500° C (Fig. 8) can be associated with normal grain growth. Abnormal grain growth, observed in the previous stage, ceases when abnormally growing grains start to impinge on each other. Their comparable sizes now produce rather flat grain boundaries, which eliminates the driving force for fast growth. The rate controlling process in grain growth can be expected to be the boundary mobility, since porosity is nearly eliminated in this stage (Fig. 6). For boundary control of grain growth, Brook [23] derives $n = 2$ to 3, depending on the extent of segregation to the boundary. Assuming the necessary segregation to keep up with the grain boundary in the previous stage of abnormal grain growth, the elementary process involving grain growth is the same in both mechanisms and the obtained value for ΔE may be used to estimate the growth exponent n, using Equation 4 and Fig. 8. This yields $n = 3$, which indicates preferential segregation in a system exhibiting normal grain growth. Indeed recent investigations in the authors' laboratory [27] have shown that the grain boundaries of $Zr_{0.85}Y_{0.17}O_{1.9515}$ ceramics are enriched in Y^{3+}.

The temperature region $1500 < T < 1600^\circ$ C again reveals a notable increase in the slope of the grain growth curve, which may be indicative of the occurrence of a second stage of abnormal grain growth. The sample sintered at 1550° C, a temperature lying in the middle of the region concerned, reveals a microstructure which is indicative of an abnormal grain growth mechanism: several areas all through the sample show the presence of strongly coarsened grains, bounded by a population of significantly smaller grain sizes. Fig. 11 gives an example of this phenomenon. Further evidence of the occurrence of abnormal growth at $< 1600^\circ$ C was found in the microstructure of samples sintered at temperatures exceeding 1600° C [1] showing pores which have become detached from grain boundaries, resulting in a coarse grained structure with small intra-granular pores. The onset of abnormal growth at 1500° C might be initiated when the previously noted impurity drag effect ceases as a result of increasing grain boundary velocity of the growing grains. Finally at 1600° C grain growth reverts back to normal when the abnormal grain boundaries impinge on each other.

3.4. Discussion of calculated activation energies

The calculated activation energy for grain growth of 450 kJ mol^{-1} must be compared with literature values, obtained from sintering experiments. Grain growth implies the diffusional jump of constituent ions across the grain boundary. According to Kingery [28], the energy of activation ΔE for

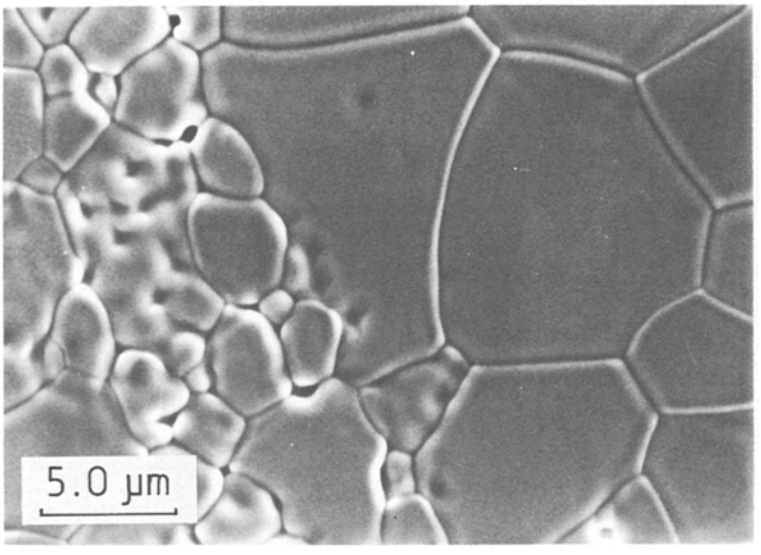

Figure 11 Scanning electron micrograph of a sample sintered at 1550° C showing anomalous growing grains.

grain growth should be intermediate between ΔE for grain boundary diffusion and lattice diffusion, and mostly approximates ΔE for grain boundary diffusion.

A literature survey shows cation diffusion to be the slowest: e.g. for lattice diffusion of Zr^{4+} and Ca^{2+} in the system $0.16\,CaO$–$0.84\,ZrO_2$, ΔE values of 387 and 421 kJ mol^{-1} respectively have been measured [29]. In the solid solution $0.16\,Y_2O_3$–$0.84\,ZrO_2$, interdiffusion experiments reveal a lattice diffusion ΔE for Zr^{4+} of 391 kJ mol^{-1}, which is insensitive to the level of dopant. For grain boundary diffusion in the same material Zr^{4+} experiences $\Delta E = 309$ kJ mol^{-1} [30]; no data on Y^{3+} diffusion are reported. The measured value of 450 kJ mol^{-1} can be regarded as an indication of Y^{3+} lattice diffusion to the be slowest process, associated with grain growth. ΔE has not been reported for Y^{3+}, but can be expected to exceed the value for Zr^{4+}, considering the larger ΔE found for Ca^{2+} lattice diffusion.

The activation energy, estimated for grain growth in the temperature region 1100 to 1200° C resembles lattice diffusion values, and not as expected grain boundary diffusion. The reason for this deviation might be the implicitly assumed independence of ΔE for grain growth on grain size. A small grain size means a small radius of curvature of the grain boundary. Consequently, at strongly curved boundaries one side will be enriched and the other side impoverished in vacancies [28]. This impoverishment may cancel out the beneficial effects of grain boundaries on diffusion. Since grain growth involves the diffusion jump of an ion from the vacancy-impoverished to the enriched side of the grain boundary, the environmental situation of the jumping ion at small grain sizes approximates more the bulk situation, and therefore ΔE approaches the value for lattice diffusion. This effect would not be noted in sintering studies, since grain growth involves material transport across the grain boundary, while sintering implies transport *along* the boundary. Thus for sintering the grain boundary, being the faster transport route, is not blocked, but merely diverted to one side of the boundary. In this respect the activation energy found can be regarded as satisfactory, and does not conflict with the proposed grain growth mechanism.

4. Conclusions

The sintering studies show that understanding and control of grain growth is of utmost importance in the whole temperature region, but especially in the lower temperature areas.

The microstructure of ceramics, produced from ultra-fine grained powders, having a *normal* grain size distribution after sintering, develops via a transient stage of *abnormal* grain growth, which is determined by the microstructural situation after compaction.

In order to achieve high density and small ceramic grain sizes at low temperatures, the stage of abnormal grain growth, between 1100 and 1200° C, should be kept as short as possible.

In the first stage of sintering, densification and

grain growth are restricted to the internal aggregate microstructure. Consequently, the originally uniform-sized primary crystallites transform into a grain size distribution which is fully determined by the original aggregate size distribution. Since the larger grains in a size distribution are the starting points for abnormal grain growth, relatively large aggregates can be seen as a serious threat to the achievement of fine-grained, dense ceramics. Efforts must, therefore, be made either to avoid the presence of (large) aggregates, or to obtain a narrow aggregate size distribution. The key to solving this problem lies in control of the agglomerates and aggregates in the starting powders.

Acknowledgements

The authors are indebted to Ing M. A. de Jongh and Dr J. Beyer for their co-operation concerning electron microscopy. Mr H. Kruidhof is acknowledged for performing several X-ray fluorescence analyses and Mr D. Wesseling for his indispensable technical assistance.

References

1. M. J. VERKERK, B. J. MIDDELHUIS and A. J. BURGGRAAF, *Solid State Ionics* **6** (1982) 159.
2. M. A. C. G. VAN DE GRAAF, T. VAN DIJK, M. A. DE JONGH and A. J. BURGGRAAF, *Sci. Ceram.* **9** (1977) 75.
3. M. A. C. G. VAN DE GRAAF, K. KEIZER and A. J. BURGGRAAF, *ibid.* **10** (1980) 83.
4. M. A. C. G. VAN DE GRAAF, J. H. H. TER MAAT and A. J. BURGGRAAF, "Ceramic Powders", edited by P. Vincencini (Elsevier Scientific Publishing Cie, Amsterdam, 1983) pp. 983–794.
5. A. J. A. WINNUBST, K. KEIZER and A. J. BURGGRAAF, *J. Mater. Sci.* **18** (1983) 1958.
6. M. A. C. G. VAN DE GRAAF and A. J. BURGGRAAF, *Advances in Ceram.* **12** in press.
7. K. S. MAZDIYASNI, C. T. LYNCH and J. S. SMITH II, *J. Amer. Ceram. Soc.* **50** (1967) 532.
8. M. HOCH and K. M. NAIR, *Ceram. Int.* **2** (1976) 88.
9. H. Th. RIJNTEN, Ph.D. thesis, Delft University of Technology, Delft, The Netherlands (1971).
10. K. HABERKO, *Ceram. Int.* **5** (1979) 148.
11. R. YU. SHEINFAIN and T. F. MAKOVSKAYA, *Koll. Zh.* **58** (1976) 816.
12. O. P. STAS', R. YU. SHEINFAIN and I. E. NEIMARK, *ibid.* **39** (177) 393.
13. M. L. VEIGA, M. VALLET and A. JEREZ, *Ann. Chim. Fr.* (1981) 341.
14. R. M. DELL and S. WELLER, *Trans. Faraday. Soc.* **55** (1959) 2203.
15. D. C. BRADLEY and W. WARDLAW, *J. Chem. Soc.* (1951) 280.
16. L. M. BROWN and K. S. MAZDIYASNI, *Inorg. Chem.* **9** (1970) 2783.
17. E. J. LYONS, "Mixing" Vol. 2, edited by V. W. Uhl and J. B. Gray (Academic Press, New York, 1967) p. 229.
18. H. KRUIDHOF, *Anal. Chim. Acta* **102** (1978) 177.
19. D. E. NIESZ, R. B. BENNETT and H. J. SNYDER, *Ceram. Bull.* **51** (1972) 677.
20. H. BOSCH and A. PEPPELENBOS, *J. Phys. E: Sci. Instr.* **10** (1977) 605.
21. D. DOLLIMORE and G. R. HEAL, *J. Appl. Chem.* **14** (1964) 109.
22. K. P. KLUG and L. E. ALEXANDER, "X-ray Diffraction Procedures" (Wiley and Sons, New York, 1974).
23. R. J. BROOK, Ceramic Fabrication Processes in "Treatise of Materials Science and Technology" Vol. 9, edited by F. F. Y. Wang (Academic Press, New York, 1976) pp. 331–364.
24. M. SAKARDAN, C. H. HSUEH and A. G. EVANS, *J. Amer. Ceram. Soc.* **66** (1983) 456.
25. R. J. BROOK, *ibid.* **52** (1969) 56.
26. M. HILLERT, *Acta Metall.* **13** (1965) 227.
27. A. J. A. WINNUBST, P. J. M. KROOT and A. J. BURGGRAAF, *J. Phys. Chem. Sol.* **44** (1983) 955.
28. W. D. KINGERY, H. K. BOWEN and D. R. ULMANN, "Introduction to Ceramics" (Wiley and Sons, New York, 1976) pp. 448–476.
29. P. KOFSTAD, "Non-stoichiometry, Diffusion and Electrochemical Conduction in Binary Metal Oxides" (Wiley and Sons, New York 1972) pp. 162–164.
30. Y. SAKKA, Y. IOSHI and K. ANDO, *J. Mater. Sci.* **17** (1982) 3101.

Received 29 May
and accepted 3 July 1984